Hindawi
International Transactions on Electrical Energy Systems
Volume 2023, Article ID 3048966, 19 pages
https://doi.org/10.1155/2023/3048966

WILEY | Hindawi

Research Article

Intentional Islanding of Active Distribution Networks by GenSets: An Analysis of Technical Constraints and Opportunities

Edoardo Daccò, Davide Falabretti, and Andrea Vicario

Department of Energy, Politecnico di Milano, Milano 20156, Italy

Correspondence should be addressed to Davide Falabretti; davide.falabretti@polimi.it

Received 31 December 2022; Revised 26 May 2023; Accepted 29 May 2023; Published 14 June 2023

Academic Editor: Mahdiyeh Eslami

The willingness to improve the security and reliability of power supply to end-users, often pushed by prescriptions of national regulatory authorities, is bringing considerable challenges for distribution system operators. Islanding a portion of the public distribution network after a fault is considered a measure to mitigate the effects of service interruptions. This procedure is usually carried out by counterfeeding the grid through a generator set (GenSet). Even if this approach is widely adopted around the world, reenergizing the grid and keeping the electric island stable is not a trivial task. In this framework, the scope of this paper is to provide a set of technical guidelines for the usage of GenSets to supply public grids in emergency conditions. The goal is to highlight the static and dynamic limits of the GenSet operations and simplify their exploitation for the grid operators. The numerical analyses, which have been carried out through the RMS simulation tool of the DigSilent PowerFactory software, also aim to evaluate the technical constraints in the case of active networks, which involve distributed generation implementing regulations according to ENTSO-E and Italian technical standards.

1. Introduction

In recent years, the global GenSets' (GSs) market size has constantly increased. In 2019, it was valued at USD 23.9 billion, and it is expected to progress at a compound annual growth rate of 8.1% over the next ten years [1]. This positive trend is supported by the growing demand for reliable and uninterrupted power supply from end-use sectors, such as construction, manufacturing, telecommunication, and power generation. In public distribution networks, GSs are adopted as an emergency power supply when a fault occurs and the main grid is unavailable. In recent years, the usage of GSs as backup generators on public distribution grids increased due to the fast spreading in the EU and worldwide of more and more challenging prescriptions for distribution system operators (DSOs) in terms of a better continuity of service, both during single fault events and in case of large accidents affecting the grid (e.g., force majeure events). Following the emergency operating practices of DSOs, this paper investigates how intentionally islanding a portion of the public distribution network supplied by a backup diesel GS could improve the continuity and quality of the electric service in a radially arranged system. In particular, the technical aspects affecting the island operation are evaluated and proper technical criteria are formulated to support the DSO in creating and managing the network supplied by the GS.

The introduction is organized as follows: in Subsection 1.1, the main motivations of the paper are explained, while in Subsection 1.2, an overview of the relevant literature, including key theoretical frameworks and relevant studies, is provided; finally, in Subsection 1.3, the innovations and original contributions of the study are outlined.

1.1. Motivation and Incitement. This paper evaluates the static and dynamic stability of a diesel GS used to supply a medium voltage (MV) distribution grid to mitigate the effects of service interruptions and guarantee a better continuity of power supply. The need for a better quality of

service is also a consequence of the regulatory schemes applied to network operators in many countries in the EU, which reward or penalize the DSO according to the level of continuity of service provided to users, measured according to the indicators defined by the technical standard EN 50160 [2]. These schemes are usually applied by defining service continuity standards ("target levels") [3], which establish a maximum number and duration of interruptions that each DSO must guarantee to its customers over a year. In general, this approach has shown in the past good results in pushing continuity of service toward better quality levels [4] and promoting the adoption of more advanced protection and automation schemes, especially over MV distribution networks. However, in grids with a purely radial layout without the possibility of reverse feeding, or in case of multiple faults, the emergency supply by a GS can be considered the only solution capable of limiting the interruption duration for the involved customers.

Moreover, in some countries, additional measures have been taken to deal with exceptional events, like those caused by large weather accidents: snowfalls, waterfloods, and windstorms. In Italy, for example, the DSOs must prepare a three-year horizon plan (so-called resilience plan) and send it to ARERA, the national energy regulatory authority, for approval [5, 6]. This plan must include a set of actions selected by the DSO to contain the risk of power outages against the main critical factors that may impact the distribution network. The effectiveness of the interventions in improving the grid operation is assessed based on their ability to increase the network robustness or to mitigate the effects of a contingency; the latter can be addressed by increasing the readiness of restoration actions using GSs as an emergency power supply. In this context, the adoption of GSs to counterfeed a portion of the distribution network working as an intentional electric island shows significant benefits; because by reducing the outage period, the customers can experience a better continuity of service. In addition, also people's safety increases, especially in environments such as mountains or rural areas, where most public networks are radially arranged, and outages could last more than a day [7]. Therefore, one of the main goals of the present paper is to investigate if following the current emergency procedures put in place by the DSOs, the intentionally islanded portion of the public distribution network is dynamically stable if supplied by a mobile GS.

Furthermore, distribution networks are undergoing a phase of deep transformation due to global drivers related to environmental issues [8]. In this new energy scenario, DSOs must face a wide diffusion of small-sized power plants [9], the so-called dispersed generation (DG), supported by a legislative framework strongly oriented toward incentives for renewables. In the near future, distributed energy resources (DERs) on MV and LV grids could also be used to manage contingencies and backup plans, especially if connected through grid-forming inverters [10–12]: by adopting a suitable control logic, they can emulate the behavior and inertia of synchronous machines, even with better performance, providing a voltage and frequency reference to the entire system. However, nowadays, a black start scheme from DG units still requires reliable power supplies and stable voltage references, which fuel-driven rotating machines (e.g., GSs) can only offer. In this scenario, the goal of the work is to carefully evaluate the interaction between the GS and DG units within an electric island. This investigation is of particular interest also because, in recent years, technical connection rules for DG units in many countries have been updated to include a minimum set of active and reactive power control functions to support the grid in contingency conditions. This is the case in Italy of technical standards CEI 0–16 and 0–21 [13, 14], which provided a set of prescriptions concerning the DG connection to the MV/LV grid, harmonized with the relevant ENTSO-E network code [15, 16].

1.2. Literature Review. In the literature, the study of the behavior of GSs as backup power supply on distribution systems is of particular interest due to their wide use motivated by the relevant robustness and reliability; for this reason, several papers study the optimal design of GSs in different operating conditions. In general, the GS must be properly sized for supplying large and varying loads, such as motors; if not so, significant stability issues (e.g., frequency and voltage fluctuations) may occur, especially during sudden load changes (e.g., motors startup) [17]. To avoid these problems, the main research and development effort by GS manufacturers is related to the design of high-performance speed governors and voltage excitation systems [18]. Concerning frequency control, the GS regulates its mechanical torque according to the power required by the load. In [19], several configurations of speed governors are presented, and their benefits on the stability of the islanded portion of the distribution network are highlighted. In [20], the authors investigate the frequency stability of the island with GSs that work both in isochronous and droop conditions; the proposed frequency control could ensure the stability of the electric grid after a major generation outage. The stability of the electric island may also be threatened by other factors, for example, according to [21], in extreme load conditions, when the electrical load torque exceeds the mechanical torque limits of the prime mover, the stalling of the GS occurs and the integrity of the island is compromised.

Even if this is not the focus of this work, it is worth mentioning that a significant area of the research related to the islanded operation of public networks aims to study unintentional electric islands. In particular, several papers define new protection strategies to avoid the unintentional islanding operation of portions of public distribution networks with high penetration of DG, for example, adopting governor signal clustering [22], fuzzy classifier or inference systems [23, 24], deep learning techniques [25, 26], rate of change of reactive power criteria [27], and Gibbs phenomenon-based hybrid methods [28]. Authors in [29, 30] propose an innovative machine learning-based anti-islanding method tested on a microgrid with a real-existing PV plant, which is compared to other islanding detention methods. All these studies highlight a strong interest from the scientific community in avoiding unwanted operating

conditions that could jeopardize the distribution grid's reliability and safety. However, this paper approaches the problem of how to guarantee a better continuity of service of the MV/LV network from a different point of view, that is, by facilitating the use of GSs to supply portions of public grids during outages and emergency conditions, manage the network as an intentional electric island.

Regarding the intentional islanding operation supported by DG units, the optimal location and sizing of a set of DG units designed to operate in a stand-alone grid in emergency conditions are studied in [31]. New approaches aiming at promoting DG units as the only power supply are also evaluated in [32–34], especially exploiting grid-forming inverters. However, as already introduced, black start schemes nowadays cannot rely yet on DG only, due to its typical uncontrollability and still limited diffusion, at least in some areas of the territory. Indeed, in the literature, some works investigate the stability of the island when both rotating machines and inverter-based dispersed generators are powering the system. For instance, in [35], the load sharing and the consequent electromechanical transients are analyzed. Moreover, the authors provide a detailed examination of the differences between the frequency-regulation characteristics of inverters and generators to explain the cause of the poor transient power sharing. Similarly, [36] studies the interaction between synchronous generator and inverter-based DG in a stand-alone grid: a modified droop control technique is proposed to improve their transient behavior during active and reactive power sharing. However, this paper does not consider the reconnection process of the DG to the island and its possible effects on its stability. In [19], the power losses calculation and short-circuits' analysis have been performed on an intentional island with GSs and wind power plants. Finally, the benefits for the stability of the system of the load sharing between different DG units, having different technology and primary source, are analyzed in [37].

As far as the authors know, a complete understanding of the interactions between the GS power controls and the DG regulation logics for grid service-related purposes is not present in the literature. Moreover, at present, there is a lack of literature studying the impact of different grid configurations on the repowering ability of commercially available GSs. This shortfall represents a significant knowledge gap that this paper wants to address to better understand the behavior of intentionally islanded grids. Hence, this study provides valuable insights into the impact of DG units on the islanded grid and can help to identify the optimal control strategies for ensuring system stability and reliability.

1.3. Goals, Contribution to the State of the Art, and Paper Organization. In the outlined framework, this paper aims to further extend the knowledge on the topic, providing a set of technical guidelines for the proper usage of backup diesel GenSets on public grids in emergency conditions. The main contributions of this paper are summarized as follows:

(i) The identification, modeling, and optimal tuning of all the components needed to faithfully reproduce the real behavior of an emergency GS during its operation, in particular concerning the speed governor and voltage excitation systems, which are crucial elements for ensuring the stability of the system, particularly when disconnected from the main grid

(ii) The development of realistic numeric models of inverter-based DG units that incorporate active and reactive power control logics for grid-purpose services aligned with both ENTSO-E and Italian technical standards

(iii) The evaluation of the static and dynamic operational limits of the GS on a wide set of electric island grid configurations to highlight the backup generator's capability and limitations

It is worth noticing that, in this paper, the variability of the input parameters, such as the characteristics of the GS or of the distribution grid, is addressed by adopting the technical characteristics of network components most widely used in real-existing applications and, when possible, by performing parametric analyses testing how different values of the same parameter change the behavior of the system. Moreover, in order to give more generality to the approach, we identified the limit conditions under which the GenSet can safely supply a portion of the isolated distribution grid. This way, the results obtained can be applied across a wide range of scenarios and electrical networks, as long as the parameters fall within those considered in the study. For these reasons, despite the variation in the numerical results, the robustness of the developed technical guidelines remains valid.

In the following, an in-depth description of the models developed for the GS components (Section 2) and of DG control laws is provided (Section 3). The case study considered to evaluate the stability limits of the electric island, and the relevant results are presented in Section 4. Then, a case study involving an active public grid is analyzed in Section 5 to understand the limits and benefits of DG in the electric island. Finally, conclusions are provided.

2. Generator Set Modeling

In the present work, a model has been developed in DigSilent PowerFactory to simulate the operation of a GS by employing the information available in the literature or provided by manufacturers (e.g., datasheets). The implemented model consists of a prime mover (i.e., a diesel motor), an alternator (i.e., a three-phase synchronous generator), a speed governor, and a voltage excitation system (Figure 1).

The diesel engine and alternator protections have not been implemented in the software environment, but they have been considered during the evaluation of the results in the different case studies.

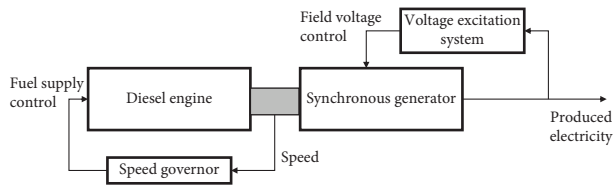

Figure 1: Block scheme of the GS model implemented.

2.1. The Alternator. In general, the alternators coupled with prime movers can be synchronous or asynchronous generators, or dynamos. In this work, a three-phase synchronous generator is considered, which is the most widely adopted solution for GSs used as emergency power supply. The static limits of operation of the GS are described by the capability curve shown in Figure 2.

In particular, the capability curve is bounded by the following limits [38]:

(i) The stator limit, defined by the maximum stator current (usually, the nominal one) to avoid overheating in the stator windings.

(ii) The rotor limit, function of the maximum excitation current to avoid overheating in the rotor windings.

(iii) The turbine limit, given by the maximum mechanical torque that can be applied to the alternator shaft.

(iv) The stability limit, corresponding to the maximum load angle allowed to avoid the loss of synchronism of the generator. Even if the loss of synchronism occurs when the load angle reaches 90°, in practice, a safety margin of 10% of the nominal power is considered, reducing this limit to 65/70° [38].

Usually, to prevent generator damage, the GS is equipped with protections that detect if the capability limits are overcome, i.e., if the operating point is outside the capability curve, and consequently trip.

2.2. The Speed Governor. The selected speed governor is a diesel Woodward model (Figure 3), used in most diesel-driven GSs [39]. It is a speed droop governor that can work both in isochronous and droop conditions, depending on the parameter D of the "droop" feedback block. In the intentional islanding operation, the isochronous condition ($D = 0$) is usually preferable because the frequency is maintained at the reference value (50 Hz). However, in some cases, a droop behavior can be preferable, especially to prevent issues in the power sharing, when more than one generator supplies the island. Therefore, in the next case studies, both control laws will be analyzed to investigate the stability of the electric island.

The "electric control box" block takes in input the speed error and provides as an output an electric signal that oscillates with a damped motion around the value of the speed error. According to the electric signal delivered, the electromechanical "actuator" block provides the output throttle, which controls the fuel injection of the diesel engine; this signal is saturated by T_{max}/T_{min} to avoid over/under fueling conditions. Finally, the "combustion delay" block represents the diesel engine's response to a variation of the throttle. The output of the model is a mechanical torque that, multiplied by the instantaneous value of the speed, provides the mechanical power P_m applied to the alternator.

2.3. The Voltage Excitation System. Regarding the voltage excitation system, the selected one is a static IEEE model (Figure 4). The choice of a static model is related to the fast time response of this exciter, the reduced axial dimensions, high reliability, and efficiency [40].

The "input filter" works as a first-order lag in which the output signal reaches the input steady-state voltage value at the generator terminals V_c after a small transient, avoiding any step change. Given the voltage error between the filtered voltage input and the reference value V_{ref}, the "regulation" block behaves as a first-order lag with a multiplication factor at the numerator. Thus, it works as an amplifier, intensifying the input signal and damping out any abrupt change within the range V_{min}–V_{max}. Then, the "excitation" block operates as a pure integrator: the input regulation voltage is converted into the excitation voltage *EFD* of the synchronous generator. When the maximum excitation voltage is reached, it is limited to EFD_{max}, which represents the physical limit on the excitation voltage due to the saturation of the magnetic components. The time constant *TE* is associated with the inductance of the control windings. The "feedback control" block works as a first-order lag differentiator: the output voltage signal V_f is the first derivative with respect to the time of the input voltage signal EFD. This derivative feedback is used to improve the dynamic response of the system. Indeed, it works as a compensation feedback signal.

All the parameters that characterize the alternator, the speed governor, and the voltage excitation system are reported in the case study description (Section 4).

3. DG Unit Modeling

Concerning the DG, today most of the dispersed units on MV/LV networks, especially from PV/wind generation, are coupled to the grid by inverters. Hence, in this work, DG has been modeled into the DigSilent PowerFactory environment as a current-controlled static generator, normally working at a unitary power factor (Figure 5). In this configuration, the "per unit" values of the direct (id_{ref}) and quadrature (iq_{ref}) axes current correspond, respectively, to the active and reactive power exchanges of the DG unit. Instead, the cosine (cos_{ref}) and sine (sin_{ref}) input signals generated by the phase-locked loop (PLL) provide the reference values to perform the park's transformation between the phasor and time domains.

The additional measurements required for proper modeling of the DG unit are provided by the "voltage measurement," and the "PQ measurement" blocks. These blocks provide the instantaneous value of voltage u, and active and reactive power, respectively, p and q; while the frequency f is given in output to the PLL. In particular, f and

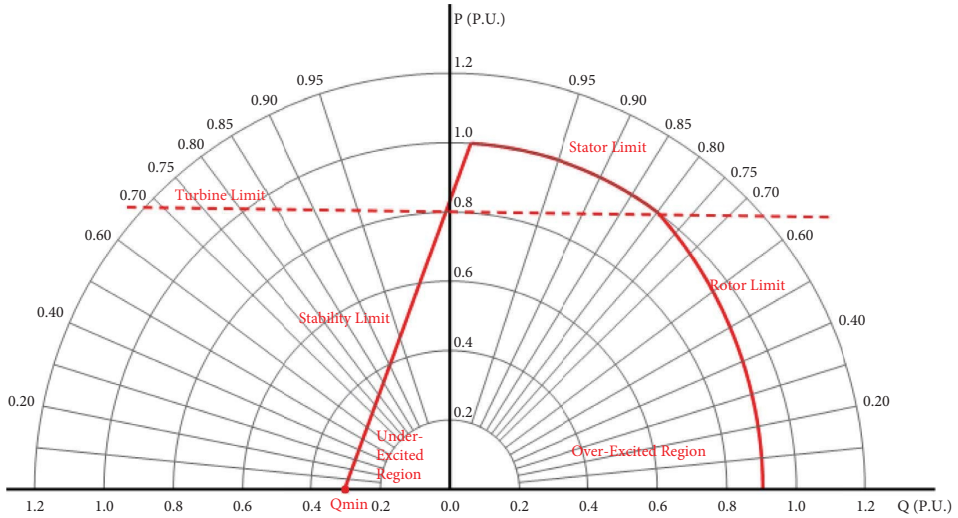

Figure 2: Capability curve of the GS. The active and reactive powers are expressed in p.u. with respect to the nominal power of the GS.

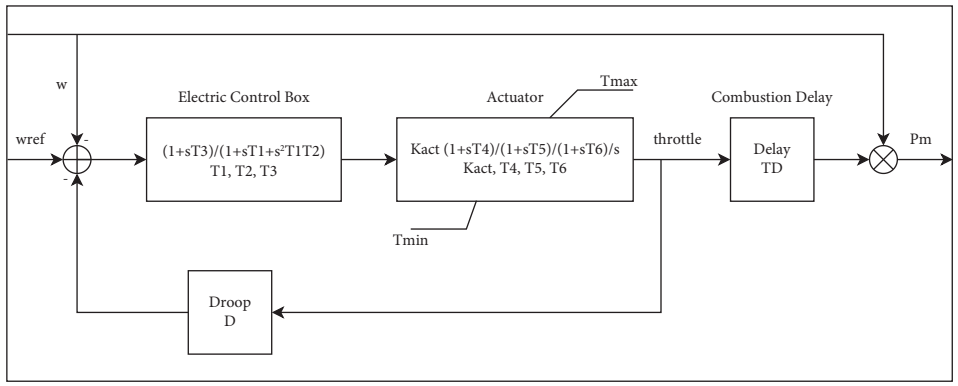

Figure 3: Woodward speed governor (DEGOV1).

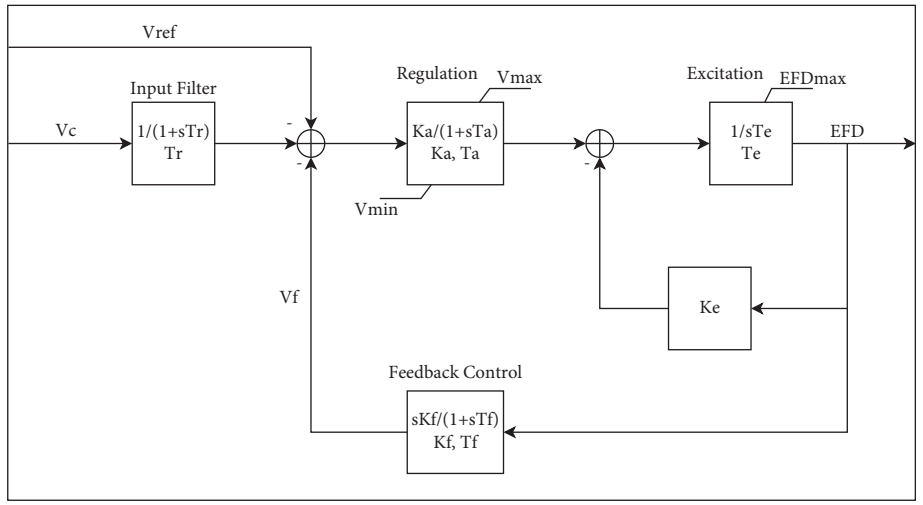

Figure 4: Static voltage excitation system (EXST2A).

p are the inputs of the "$P(f)$ regulation" block, which controls the direct axes current id_{ref}. p, q, and u are the input of the "Q(V) regulation" block, which controls the quadrature axes current iq_{ref}. These blocks model the grid service-related control logics; they are described in detail in the following paragraphs.

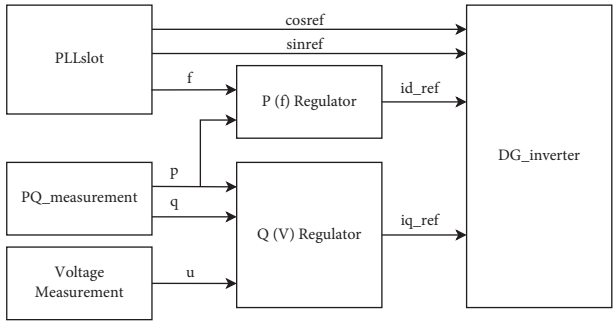

Figure 5: Block scheme adopted for the DG units (composite model).

3.1. Soft Start Ramp-Up DG Reconnection and P(f) Control Logic. According to technical standards CEI 0–16 and 0–21, a DG unit can reconnect to the MV/LV grid only if the frequency and voltage remain inside the following ranges for 100 ÷ 900 s (default time: 300 s):

(i) $85\%V_n < \mathrm{V} < 110\%V_n$

(ii) $49.00 \div 49.90\ \mathrm{Hz} < f < 50.10 \div 51.00\ \mathrm{Hz}$ (adjustable range)

In addition, the reconnection process must be gradual, performing for the active power a soft start ramp-up with a slope that should not exceed 20% of the maximum power ($P_{\max}$) of the DG unit over a minute; therefore, the complete reconnection process should last at least 300 s. The soft start aims to avoid possible disturbances and detrimental effects on the stability of the electrical grid caused by the DG.

In addition, in order to limit the extent of overfrequency events, the ENTSO-E grid code introduced a $P(f)$ control logic that modulates the active power injected into the grid by the DG unit, as reported in Figure 6. The active power is decreased linearly when the frequency exceeds a specific frequency threshold (LIf), while it is zeroed when the frequency reaches $\mathrm{Lf}_{\max}$. This control logic is only activated if DG active power is greater than a lock-in value (*LIp*).

This work implements the soft start ramp-up DG reconnection process and the $P(f)$ control logic inside DigSilent PowerFactory according to the block diagram in Figure 7. It takes as inputs:

(i) The DG bus frequency acquired by the PLL block f (Hz)

(ii) The DG active power acquired by the measurement power block p (p.u.)

(iii) The input step change of the direct axes current *yi_id* (-)

It outputs the direct axes current id_{ref} (p.u.).

The first two inputs, f and p, are processed in the "comparator" block: in order to activate the $P(f)$ regulation by the *switch* signal, both f and p must be respectively greater than *LIf* and *LIp*. *p_reg* is the active power provided by the DG unit according to the $P(f)$ characteristic (Figure 6), which is implemented through the linear "$P(f)$ lookup table." The inputs of the "$P(f)$ lookup table" are f and *pi*max; *pi*max is equal to the maximum power delivered by the DG unit when *LIf* is reached. *o_id* (and the integrator block 1/sT) is responsible for the soft start ramp-up process, which is performed by varying as a ramp signal id_{ref}.

3.2. The Q(V) Control Logic. The reconnection process of a DG unit could reverse the power flow over the grid, increasing the voltage at the DG connection point. In order to cope with this issue, a Q(V) control logic has been introduced in the technical connection rules for DG units, which adjust the local reactive power exchange as a function of the voltage measured at the point of common coupling with the grid, as Figure 8 shows. The reactive power regulation is activated if the voltage amplitude is outside the range $V1i \div V1s$. Instead, if the voltage value is outside the range $V2i \div V2s$, the regulation saturates at $\pm Q_{\max}$. According to technical standards, a rectangular-shaped capability curve has been considered, where $Q_{\max}$ is defined as 0.4843 of $P_{\max}$.

The Q(V) control logic has been modeled in DigSilent PowerFactory according to the block diagram shown in Figure 9, taking as inputs:

(i) The voltage amplitude at the DG bus u (p.u.)

(ii) The active power exchanged by the DG p (p.u.)

The output of the transfer function is the quadrature axis current iq_{ref} (p.u.).

The Q(V) control logic is activated when the active power p is greater than the lock-in value LI. This check is performed by the "comparator" block. If so, the *switch* shifts its input position from *Q_nr_pu*, which is a constant value equal to zero with a unitary power factor, to Q_ref. The latter value is defined by the "Q(V) lookup table" block, which models the Q(V) characteristic and returns as output the corresponding value of reactive power Q_ref defined according to the measured voltage amplitude u (Figure 8).

All the parameters that characterize both the $P(f)$ and Q(V) control logics are reported in Section 5.

4. Intentional Islanding Operation: Case Study Definition and Numerical Results

The case study under investigation is introduced by looking at the emergency operating practice of DSOs in a radially-arranged distribution system (Figure 10). After the occurrence of a fault on the network, e.g., on a MV line or in a MV/LV substation, the following operations are performed (as shown in Figure 10):

(i) In order to isolate the fault, the DSO usually opens the circuit breaker in the primary substation and a sectionalizing switch along the MV line

(ii) A portion of the public distribution network remains deenergized; being it radially arranged, no other paths are supposed to exist to feed MV/LV loads

(iii) In the meantime that the fault is repaired, the DSO resupplies the isolated grid by a GS connected to the

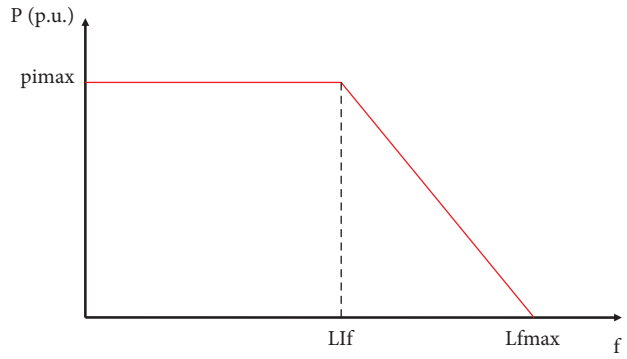

Figure 6: $P(f)$ control logic characteristic.

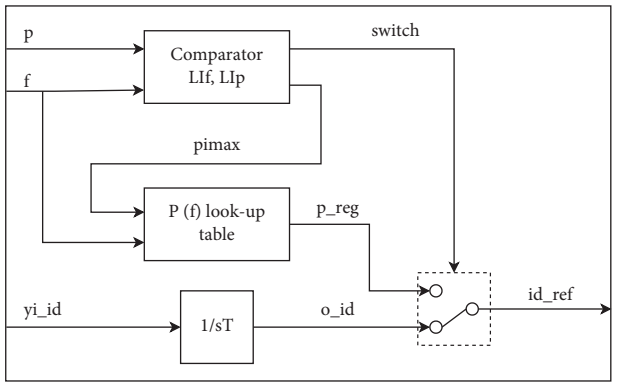

Figure 7: Common model of the soft start ramp-up DG reconnection and $P(f)$ control laws.

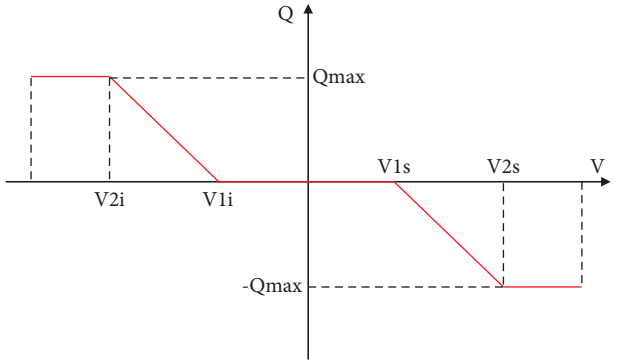

Figure 8: Q(V) control logic characteristic.

LV side of a secondary substation, thus performing an intentional islanding of the grid [41]

In DigSilent PowerFactory, this procedure has been implemented by means of the following simulation events:

(i) The test grid is deenergized at the beginning of the numerical simulation ($t = 0$ s)

(ii) At $t = 5$ s, the isolated portion of the distribution network is reenergized through the GS connected at the LV side of a secondary substation

Furthermore, the elements and parameters of the distribution test grid have been defined to recall the structure of a real-existing network. In particular, in the software

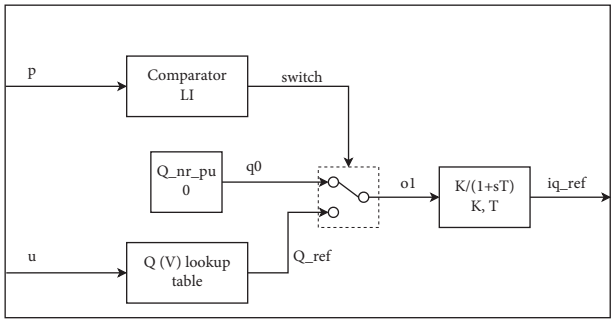

Figure 9: Common model of the Q(V) control logic.

environment, the islanded system consists of a 630 kVA MV/LV transformer (Table 1), a MV line, and a MV load.

For broader considerations on the stability of the electric island, a wide set of analyses have been performed, varying the typology (see Table 2) and length of the MV line ($0 \div 15$ km, with a step of 0.5 km), as well as the amount of load supplied, from no-load to full-load condition, with a step of 3% the nominal active power of the GS.

In Table 2, naked conductors are often used for overhead lines especially in rural areas, while cables can be used both in underground or overhead laying conditions. The 25 mm^2 cross section has been selected because it is widely adopted for terminal sections of MV lines, the most likely to be supplied through GSs.

Concerning the load behavior, a hybrid model has been considered with 50% static and 50% PQ load. This assumption has been introduced to mimic the actual load behavior in real-existing distribution networks [42].

(i) The static model considers the load as a constant impedance; therefore, active and reactive powers vary with the square of the voltage magnitude [43], as the next formulas suggest:

$$\begin{cases} P_{\text{load}} = P_{\text{rated}} \cdot \left(\dfrac{V_{\text{load}}}{V_n}\right)^2, \\ Q_{\text{load}} = Q_{\text{rated}} \cdot \left(\dfrac{V_{\text{laod}}}{V_n}\right)^2, \end{cases} \tag{1}$$

where $P_{\text{load}}/Q_{\text{load}}$ represent the actual active/reactive power required by the load, $P_{\text{rated}}/Q_{\text{rated}}$ represent their rated values, V_{load} and V_n, respectively, the voltage measured at the connection point and its nominal value.

(ii) The PQ model represents the load as a constant power bus; thus, its active and reactive powers do not depend on voltage magnitude variations as, for example, inverter-supplied loads.

The electrical and mechanical parameters adopted for the alternator are reported in Table 3.

A common size for GSs adopted in emergency conditions by DSOs has been selected for this purpose. In Table 3, the impedance values are expressed as a percentage of the reference impedance Z_{ref}:

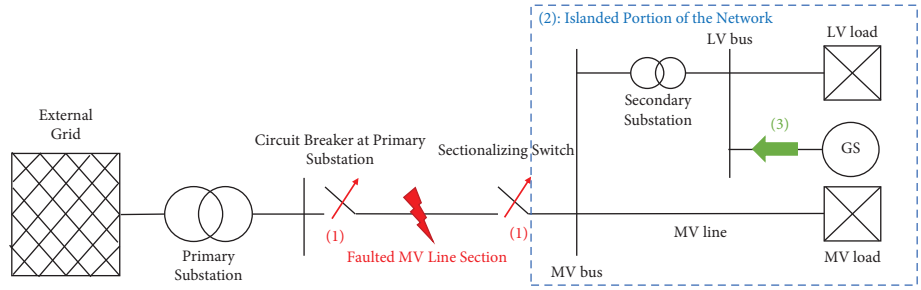

Figure 10: Schematic representation of a portion of the distribution network supplied by a GS.

Table 1: MV/LV transformer parameters.

Transformer parameter	Implemented value
Rated apparent power (kVA)	630
Rated primary side voltage (kV)	20
Rated secondary side voltage (kV)	$0.4 \pm 5 \times 2.5\%$
Vector group	Dyn5
Short circuit voltage (%)	6
Copper losses (kW)	3.20
No load current (%)	0.17
No load losses (kW)	1.09

Table 2: Naked conductors and cable MV line parameters.

Line typology	Material	Cross section (mm^2)	Resistance (Ω/km)	Reactance (Ω/km)	Susceptance (μS/km)
Naked conductor	Cu	25	0.7271	0.4213	2.780
Cable	Cu	25	0.9290	0.1500	56.548

Table 3: Electrical and mechanical parameters of the alternator.

GenSet parameter	Implemented value
Rated apparent power An (kVA)	400
Rated voltage Vn (V)	400
Rated power factor	0.8
Rated active power P_n (kW)	320
Poles	4
Direct axis synchronous reactance X_d (%)	330
Quadrature axis synchronous reactance Xq (%)	175
Direct axis transient reactance X_d' (%)	29.5
Direct axis subtransient reactance X_d'' (%)	13.2
Quadrature axis subtransient reactance X_q'' (%)	15.6
Negative sequence reactance $X2$ (%)	14.4
Zero sequence reactance $X0$ (%)	3.3
Open circuit time constant $T_{do}^{'}$ (s)	1.6
Transient time constant T_d' (s)	0.145
Subtransient time constant T_d'' (s)	0.014
Armature time constant T_a (s)	0.018
Moment of inertia J (kg·m^2)	4.8

$$Z_{ref} = \frac{V_n^2}{A_n} = 0.4\ p.u. \tag{2}$$

The parameters selected for the speed governor and voltage excitation system are reported in Tables 4 and 5.

The dynamic stability of the electric island was verified through the RMS simulation tool of the DigSilent PowerFactory software, employing a variable step size of 0.01 s. In the software environment, the electric grid was modeled as a set of differential and algebraic equations describing the behavior of the system components, including generators, transformers, lines, and loads; by solving these equations over a selected simulation period, the dynamic behavior of the islanded system was evaluated. The simulation parameters used in the analyzed case study (Table 6) were set to observe the complete electromechanical transient of all the electrical quantities. The total number of simulations performed was 3842, with a computational time for each simulation of around 0.5 s. Simulations were performed on a 12th Generation Intel(R) Core(TM) i7-1255U, CPU 1.70 GHz, RAM 16 GB computer.

4.1. Numerical Results: Dynamic Stability in No-Load Condition. In this section, the aim is to analyze the stability of the electric island during the power supply restoration process. A first set of simulations has been carried out assuming that no MV/LV loads are supplied. This assumption is coherent with the procedures carried out by DSOs: after a fault, the DSO usually finds it convenient to reenergize the grid by the GS initially in no-load conditions. This procedure is performed by powering the distribution feeder up to the MV side of the MV/LV substations and, only after, by

Table 4: Speed governor parameters.

Parameter	Value
Actuator gain Kact (p.u./p.u.)	8
$T4$ (s)	0.15
$T5$ (s)	0.1
$T6$ (s)	0.12
Combustion delay TD (s)	0.01
Droop D (p.u.)	0/0.04
$T1$ (s)	0.1
$T2$ (s)	0.008
$T3$ (s)	0.05
Minimum throttle T_{MIN} (p.u.)	0
Maximum throttle T_{MAX} (p.u.)	1.25

Table 5: Static voltage excitation system parameters.

Parameter	Value
Measurement delay t_r (s)	0.02
Controller gain K_a (p.u.)	60
Controller time constant T_a (s)	0.02
Exciter time constant T_e (s)	0.03
Exciter constant K_e (p.u.)	0
Stabilizer gain (p.u.)	0.03
Stabilizer time constant T_f (s)	0.5
Controller output minimum $V_{r\min}$ (p.u.)	−10
Controller output maximum $V_{r\max}$ (p.u.)	10
Exciter maximum output EFD_{max} (p.u.)	4

Table 6: Simulation parameters of the RMS simulation tool of the DigSilent PowerFactory software.

Simulation parameter	Value
Integration step size: electromechanical transients (s)	0.003
Integration step size: maximum step size (s)	0.01
Simulation period (s)	40

gradually reconnecting the underlying loads. In this scenario, a main problem is represented by the capacitive contribution of MV line susceptance, which is not compensated by any inductive load. Indeed, by increasing the length of the feeder, the operating point of the GS moves to the underexcited region of the capability curve toward the stability limit $Q_{\min}$ (see Figure 2), defined as follows:

$$Q_{\min} = -\frac{V_c^2}{X_d}, \tag{3}$$

where Vc represents the voltage at the GS terminals and X_d is the direct axes synchronous reactance. From data reported in Table 3, the value of $Q_{\min}$ obtained is equal to −0.12 Mvar.

The capacitive contribution is much higher for cable lines than for overhead ones (see Table 2). For this reason, they show a very different behavior when energized by a GS. In particular, naked conductor lines did not face stability issues in the whole range of the lengths considered (i.e., $0 \div 15$ km) because their capacitive contribution is low and $Q_{\min}$ is never reached over a given length. On the contrary, cable lines can cause the operating point of the GS to exceed the stability limit defined by the capability curve. If this occurs, protections trip and the electric island is deenergized. In Figure 11, the stability limit $Q_{\min}$ (red vertical line) and the operating points for different cable lengths and sections are represented. For a 25 mm^2 cable line, when the length overcomes 5 km, the reactive power produced by the feeder exceeds $Q_{\min}$, the GS is no longer able to work in stable conditions, and the system diverges. In addition, also the operating points of 95 mm^2 and 185 mm^2 cable lines are represented; their electrical parameters are reported in Table 7. It has been observed that, by increasing the section of the cable, the capacitive contribution increases as well, and the stability limit $Q_{\min}$ is reached for lower lengths; in particular, the stable length is reduced to 4 km for the 95 mm^2 and 3 km for the 185 mm^2 cable line. When the length is zero, the losses of the 630 kVA MV/LV transformer are responsible for the small amount of active power (1.09 kW) produced by the GS.

For example, Figure 12 reports the frequency and voltage measured at the GS terminals for an MV cable line (6 km long, 25 mm^2); in real-existing networks, the voltage/frequency protections mounted on the GS would immediately trip, disconnecting the GS and deenergizing the entire grid.

4.2. Numerical Results: Dynamic Stability Close to the Full-Load Condition. This scenario aims at studying the intentional island stability when the GS supplies a feeder of the public distribution network and the relative MV/LV loads. The power required by the hybrid load is such that the GS is working near the full-load condition ($87 \div 100\%$ P_n). Unlike the previous scenario, the inductive contribution of the load, which operates at a power factor equal to 0.9, compensates the line capacitance, increasing the length of the lines that can be energized both in isochronous and droop conditions, as shown in Table 8:

Regarding the isochronous condition, Table 8 shows that if the active power required by the load does not exceed 93% of the GS nominal one, the cable length that can be reenergized is more than 10 km. In this case, the intentional island stability is limited by the practical stability angle: as for the no-load scenario, when the grid extension increases, the capacitive contribution increases as well, and the operating point moves toward the underexcited region of the capability curve. Consequently, the load angle increases, getting closer to the practical stability limit (65/70°), as shown in Figure 13.

On the other hand, Table 8 shows a severe length reduction when the active power required by the load exceeds 93% of the GS nominal one. In full-load conditions, the energy losses over the MV line can bring the speed governor to work close to its saturation limits. In particular, if the frequency error is high enough to saturate the throttle signal at $T_{\max}$ (1.25 p.u.), the mechanical torque cannot compensate for the frequency deviation and the electric island frequency diverges. Figure 14 shows the MV line lengths that allow operating the network in a stable condition in the case of a 100% P_n load: the load angle is much lower than the practical stability limit, while the throttle is close to the reference value in p.u. An additional increase in the line length would saturate the throttle signal at $T_{\max}$.

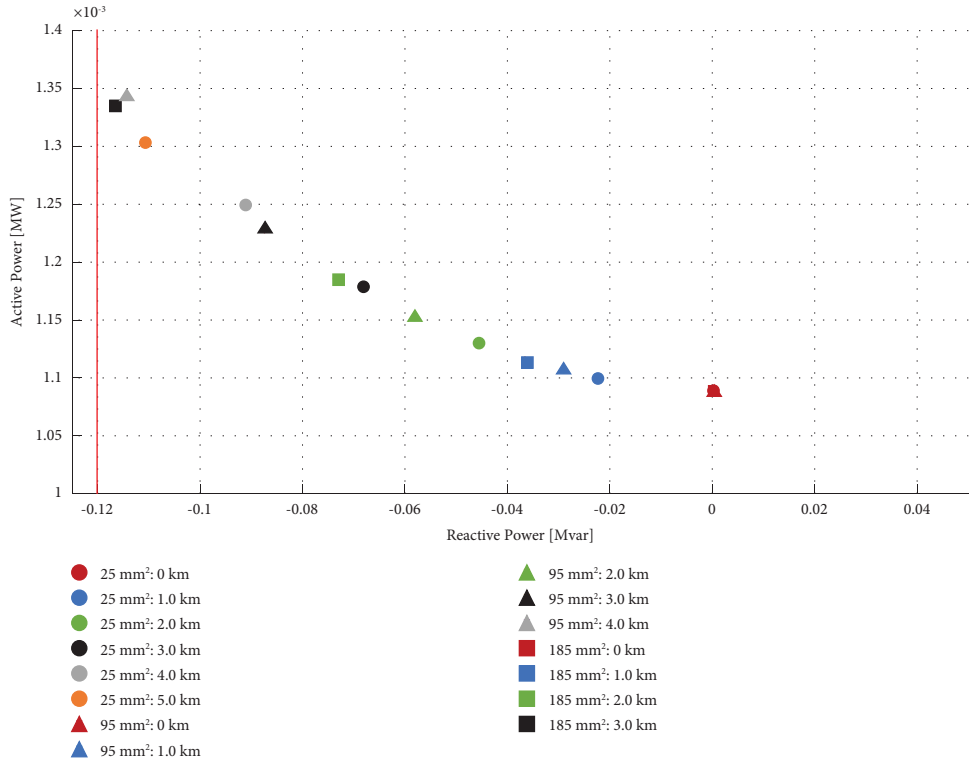

Figure 11: Capability curve—no-load condition—25/95/185 mm^2 cable line.

Table 7: 95 and 185 mm^2 cable line parameters.

Material	Cross section (mm^2)	Resistance (Ω/km)	Reactance (Ω/km)	Susceptance (μS/km)
Cu	95	0.4110	0.1200	72.257
Cu	185	0.2110	0.1100	91.106

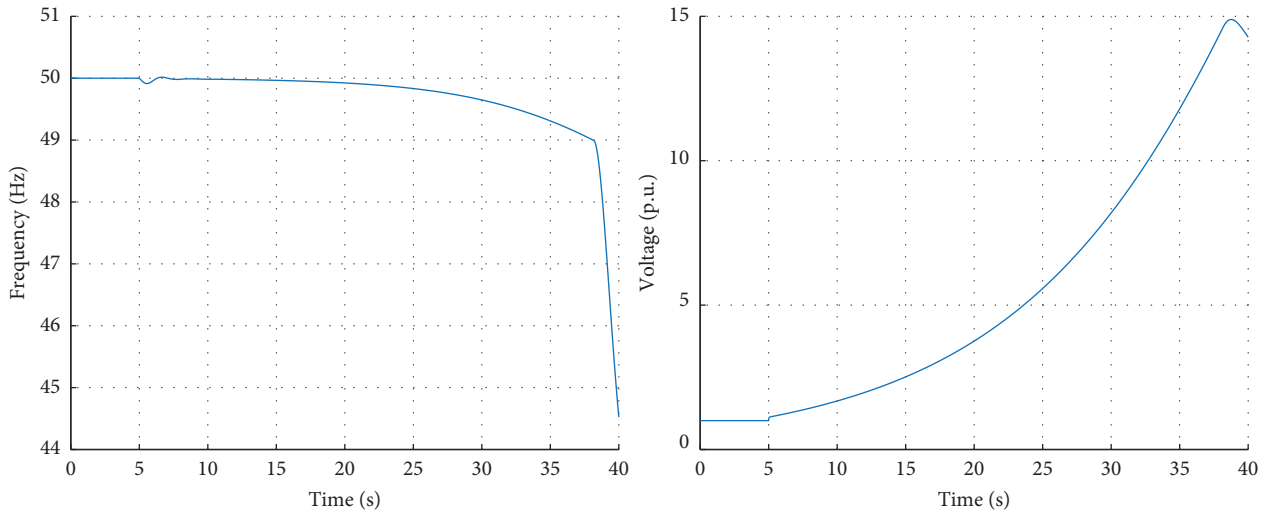

Figure 12: Frequency and voltage of the electric island in an unstable condition (6 km 25 mm^2 cable line).

For a complete understanding of possible issues affecting the stability of the electric island, a droop characteristic is also implemented on the speed governor. In particular, a 4% droop is selected (see Figure 15), assuming that the nominal frequency value (50 Hz) is reached when the GS delivers half the nominal power (0.5 p.u.). In real life, the slope and the initial frequency value of the droop characteristic can be set by the manufacturer or user of the GS.

Table 8: Length of MV cable line that can be supplied without stability issues for different load conditions in the isochronous and droop cases.

Load power ((%)P_n)	Max. length (km)—isochronous case	Max. length (km)—droop case
87	15.0	15.0
90	15.0	13.5
93	11.0	9.0
97	6.0	4.5
100	2.0	0

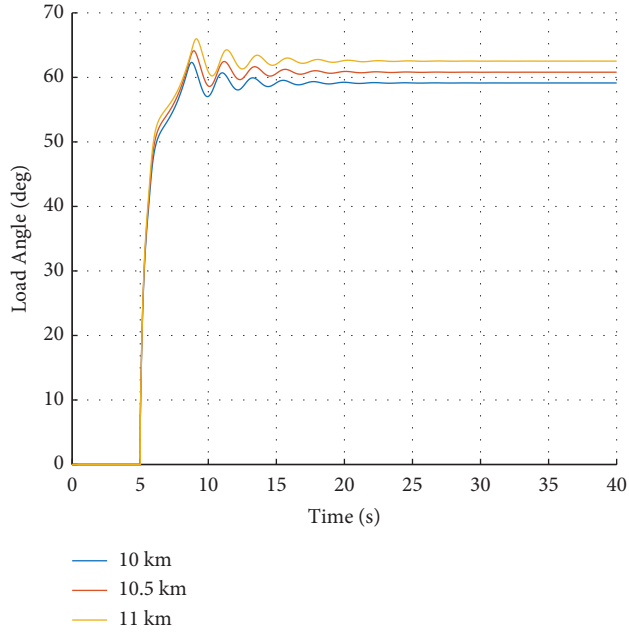

Figure 13: Load angle—90% P_n load—25 mm^2 cable line.

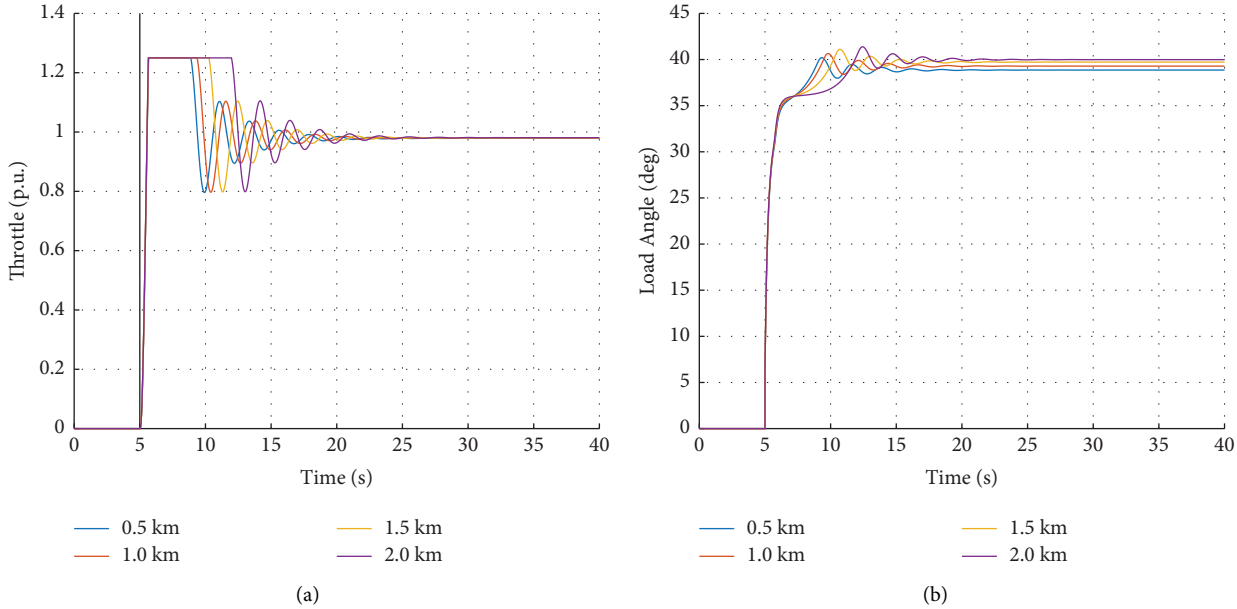

Figure 14: Throttle (a) and load angle (b) with a 100% P_n load.

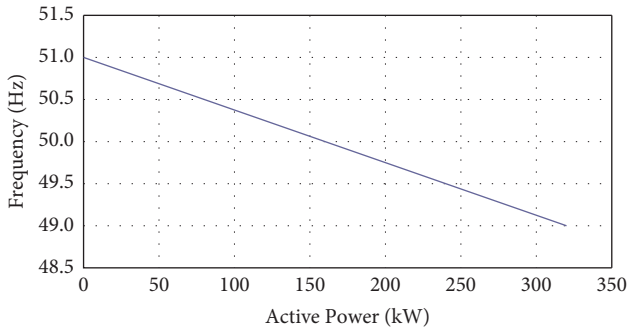

Figure 15: Selected droop equal to 4% represented in a frequency vs. active power graph.

According to the characteristic selected, in full-load condition, the frequency of the system reaches values around 49 Hz (0.98 p.u.), far below the nominal value, as shown in Figure 16.

The numerical simulations performed show that the droop characteristic reduces the maximum extension of the MV grid that can be supplied without stability issues compared to the isochronous case (Table 8, right column).

This behavior can be explained by the expression of the mechanical power P_m in output to the speed governor, which in steady-state conditions must be equal to the active power absorbed by the load:

$$P_m = T_m \bullet f. \tag{4}$$

With the droop characteristic, being the frequency lower than the nominal value, the mechanical torque Tm must increase to provide the same mechanical power P_m. Thus, T_m saturates, creating stability issues for smaller lengths of MV lines. In Figure 17, the different trend of the mechanical torque T_m is represented for the isochronous and droop conditions for the same line length (8 km).

In conclusion, the analyses performed showed that, if the distribution power system is made by cable lines, additional attention must be paid to not exceeding the maximum line length allowed by the GS capability limit. This aspect can become critical especially if the rating of the generator is similar to the active power required by loads. In this case, the admissible extension of the intentional island to prevent stability issues is drastically reduced. Finally, the adoption of a droop characteristic for the speed governor can negatively affect the maximum network extension that can be safely supplied.

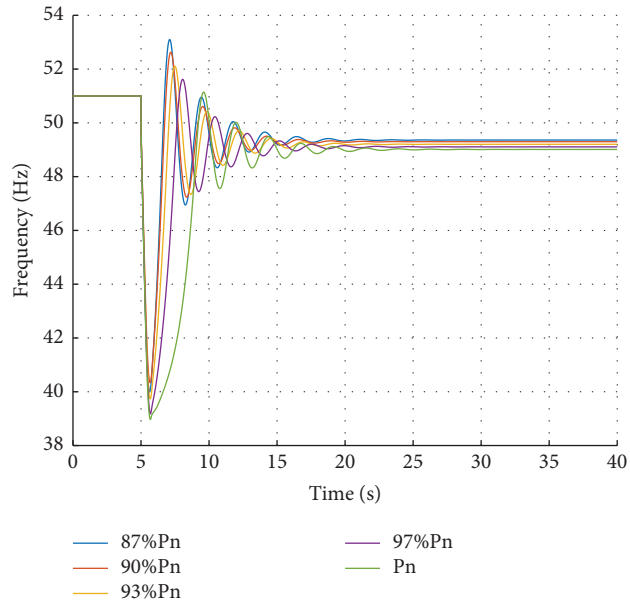

Figure 16: Frequency profile with different power required—droop condition.

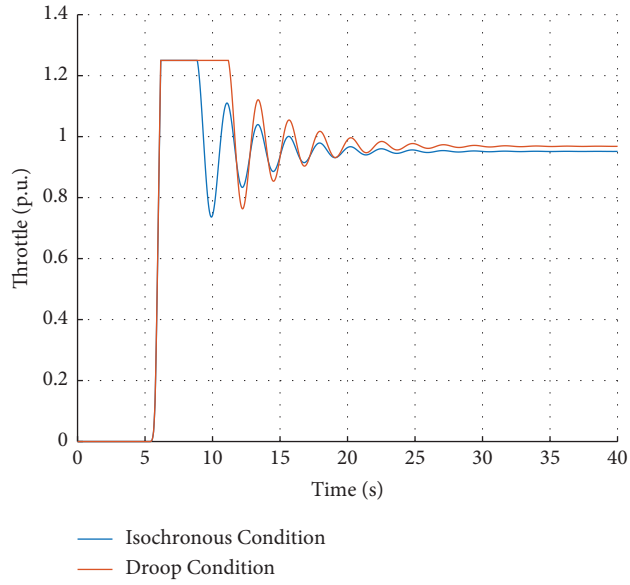

Figure 17: Mechanical torque in isochronous and droop conditions, load equal to 93% P_n of the GS, and length of the cable line 8 km.

5. Active Network: Case Study Definition and Numerical Results

The intentionally islanded portion of the public distribution network repowered by the GS may also contain DG units (Figure 18). When a fault occurs on the grid, in order not to interfere with the procedures put in place by the DSO to reenergize the faulted portion of line, the DG units are promptly disconnected. Then, once the electric island is steadily resupplied by the GS, the DG units reconnect, usually automatically. This in Italy is carried out according to the soft start ramp-up reconnection prescriptions reported in Section 3.1.

In the numerical simulations performed in the present paper, the reconnection process has been modeled by means of the following events:

(i) At $t = 0$ s: the GS is assumed to be stably counter-feeding the electric island

(ii) At $t = 100$ s: since both voltage and frequency at the terminals of the DG unit are inside the selected reconnection ranges ($85\% V_n < V < 110\% V_n$;

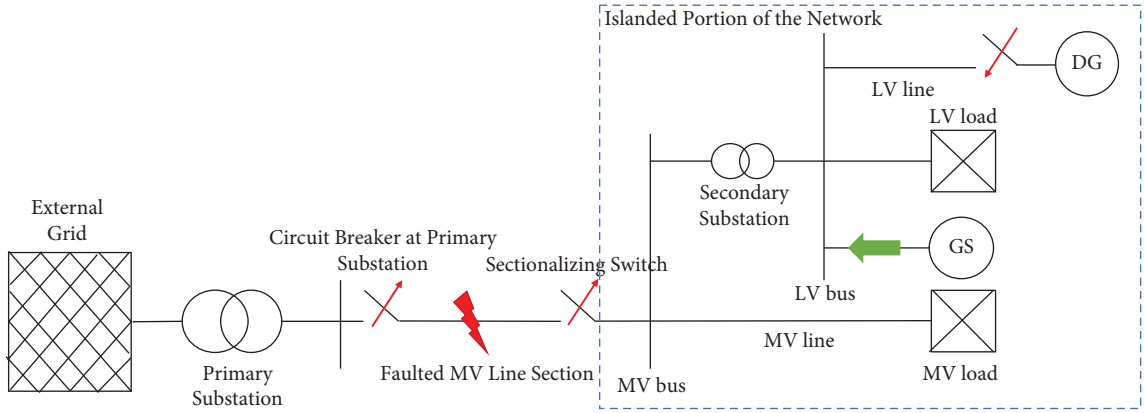

Figure 18: Schematic representation of a distribution network in presence of a DG unit connected at the LV busbar.

49 Hz < f < 51 Hz), the DG automatic reconnection process occurs and the load sharing between the GS and the DG unit starts

(iii) At $t = 400$ s: the reconnection process ends, and both GS and DG units are energizing the system

The DG unit is assumed to reconnect following a ramp-up of active power with a slope equal to +20% P_{max}/min. Therefore, the complete reconnection process lasts 300 s, as shown in Figure 19.

In this case study, the DG unit is supposed to inject a maximum power P_{max} equal to 200 kW with a unitary power factor. It is connected to the LV busbar through a LV cable line having the parameters described in Table 9 and a length equal to 0.3 km. All the other elements and the configuration of the test grid are the same as in the previous case study.

In addition, the MV load has the characteristics in Table 10.

After the reconnection of the DG unit, if voltage and frequency overcome the thresholds reported in Tables 11 and 12, the $P(f)$ and Q(V) control laws are switched on, and their effects on the electric island stability must be evaluated. By setting LIp in Table 11 equal to zero, the $P(f)$ regulation is activated regardless of the value of active power delivered by the DG unit.

As for the case study discussed in Section 4, the dynamic stability of the electric island during the reconnection process of a DG unit was investigated through the RMS simulation tool of DigSilent PowerFactory software. The simulation parameters are the same reported in Table 6, except for the simulation period, which was set equal to 500 s to observe the complete electromechanical transient of all the electrical quantities and the ramp-up process of the DG. The computational time for each simulation was around 5 s.

5.1. Numerical Results: Dynamic Stability during the DG Unit Reconnection Process. The first objective of the numerical simulation in this section was to evaluate if the automatic DG reconnection process can compromise the stability of the electric island. The most obvious effect of the DG

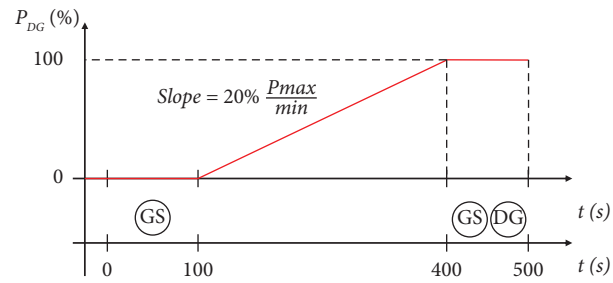

Figure 19: Reconnection ramp-up and timeline events.

injections concerns the active power balance. Indeed, if the active power provided by DG overcomes the load demand, instability will occur (Figure 20), and the active power in excess must be absorbed by the GS, causing the alternator to work as a motor. Usually, a directional relay protection is adopted on the GS to avoid this condition [39].

5.2. Numerical Results: Effects of the P(f) Control Logic. Usually, no particular issues can emerge when the $P(f)$ control logic is enabled on the DG if an isochronous speed control characteristic is adopted for the GS. In fact, the GS regulates the frequency on the grid at 50 Hz, preventing the DG from performing the $P(f)$ regulation. However, problems can arise if a droop characteristic is adopted for the GS because the frequency variation can trigger the activation of the $P(f)$ control logic. This situation is analyzed in the following simulations, where the droop characteristic reported in Figure 15 is adopted.

As described above, the GS is assumed to supply the electric island in a steady-state condition at the beginning of the simulation. According to the power requested by the load in Table 10, the frequency is equal to 49.36 Hz (Figure 21(a)). When the DG is reconnected to the grid ($t = 100$ s), the frequency increases due to the load-sharing effect between the GS and DG: the active power provided by the DG unit increases as a ramp, progressively reducing the active power that the GS supplies to the load. Consequently, the GS detects a gradual load reduction and the frequency increases following the droop characteristic of the speed governor.

Table 9: Cable LV line parameters.

Line typology	Material	Cross section (mm^2)	Resistance (Ω/km)	Reactance (Ω/km)	Susceptance (μS/km)
LV cable line	Cu	185	0.0991	0.110	0.600

Table 10: MV load characteristic in the active network case study.

Parameter	Value
P (MW)/(p.u.)	0.25/0.62
Cos (phi)	0.9-inductive
Typology	Hybrid

Table 11: $P(f)$ control logic parameters.

Parameter	Value
LIf (Hz)	50.2
Lf_{max} (Hz)	51.5
LIp (p.u.)	0

Table 12: Q(V) control logic parameters.

Parameter	Value
$V2i$ (p.u.)	0.90
$V1i$ (p.u.)	0.95
$V1s$ (p.u.)	1.05
$V2s$ (p.u.)	1.10
Q_nr_pu (p.u.)	0
K (p.u.)	1
T (s)	1
LI (p.u.)	0.2

If the $P(f)$ control logic is switched off, the active power provided by the DG unit increases according to the soft start ramp-up characteristic in Figure 19, reaching its maximum value (0.2 MW) at 400 s (blue characteristic in Figure 21(b)). At the end of the transient, the frequency is equal to 50.6 Hz (blue characteristic in Figure 21(a)).

On the contrary, if the $P(f)$ control logic is switched on, when the *LIf* threshold (50.2 Hz) is reached ($t = 300$ s), the control logic modulates the DG active power, reducing the overfrequency variation. The overlapping of this regulation with the ramp-up reconnection one results in the active power injected by the GS, which remains constant at 0.135 MW ($t = 300$ s) (orange curve in Figure 21(b)). Similarly, the frequency is also kept constant at 50.2 Hz, according to the $P(f)$ control logic shown in Figure 6.

Regarding the GS, Figure 22 shows that the active power produced by the diesel GenSet is reduced by the same amount provided by the DG unit (in this case, 0.135 MW), while the reactive power is almost constant because the DG unit is working at a unitary power factor.

Therefore, from the analyses carried out, it emerges that the $P(f)$ control logic has no detrimental effects on the proper operation of the electric island and indeed it is beneficial in mitigating possible overfrequencies: once activated, the DG active power modulation helps to keep the frequency of the system at *LIf* (50.2 Hz), avoiding further increases that could lead to protections tripping. Nevertheless, the $P(f)$ control logic has also an economic drawback for DG owners, given by the production curtailment during its activation.

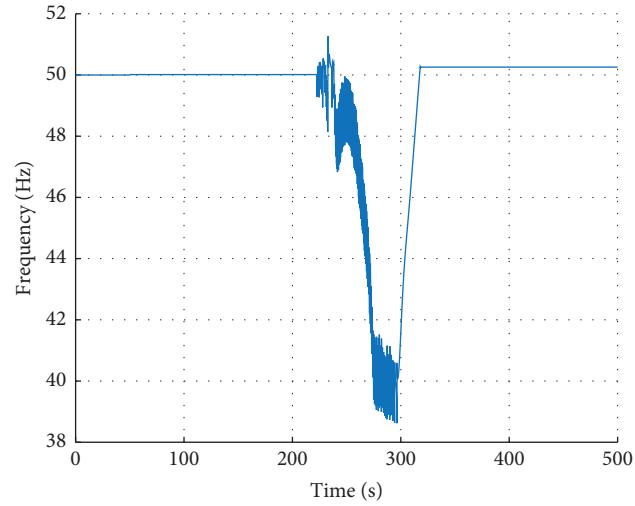

Figure 20: Frequency trend in case of active power provided by the DG unit higher than the power requested by the load.

5.3. Numerical Results: Effects of the Q(V) Control Logic. The DG reconnection at $t = 100$ s causes the reverse power flow over the LV line, thus increasing the voltage at the DG terminals with a trend similar to the reconnection ramp. When the Q(V) control logic is switched off, the steady-state voltage value at the DG unit terminals reaches 1.064 p.u., as represented by the blue curve in Figure 23(a), on the left. Instead, if the Q(V) control logic is activated, as expected, the final voltage value is closer to the reference one. According to Figure 8, when voltage overcomes $V2i$ ($t = 320$ s), the DG unit starts absorbing reactive power from the grid to compensate the voltage increase. As a result, the voltage keeps increasing but with a lower slope, which is shown by the orange curve in Figure 23(a), until that the reconnection process ($t = 400$ s) is accomplished. The steady-state voltage value is 1.058 p.u, reduced by 0.06 p.u. compared to the previous case.

This finding is confirmed by Figure 23(b): when the $V2i$ threshold is exceeded, the DG starts exchanging an amount of reactive power that is a function of the Q(V) characteristic (Figure 8). The final value of reactive power absorbed by the DG unit is 0.015 Mvar. In the simulations performed, this control logic showed to have beneficial effects on the GS operation. Indeed, the reactive power provided by the GS approaches zero, moving the operating point away from the

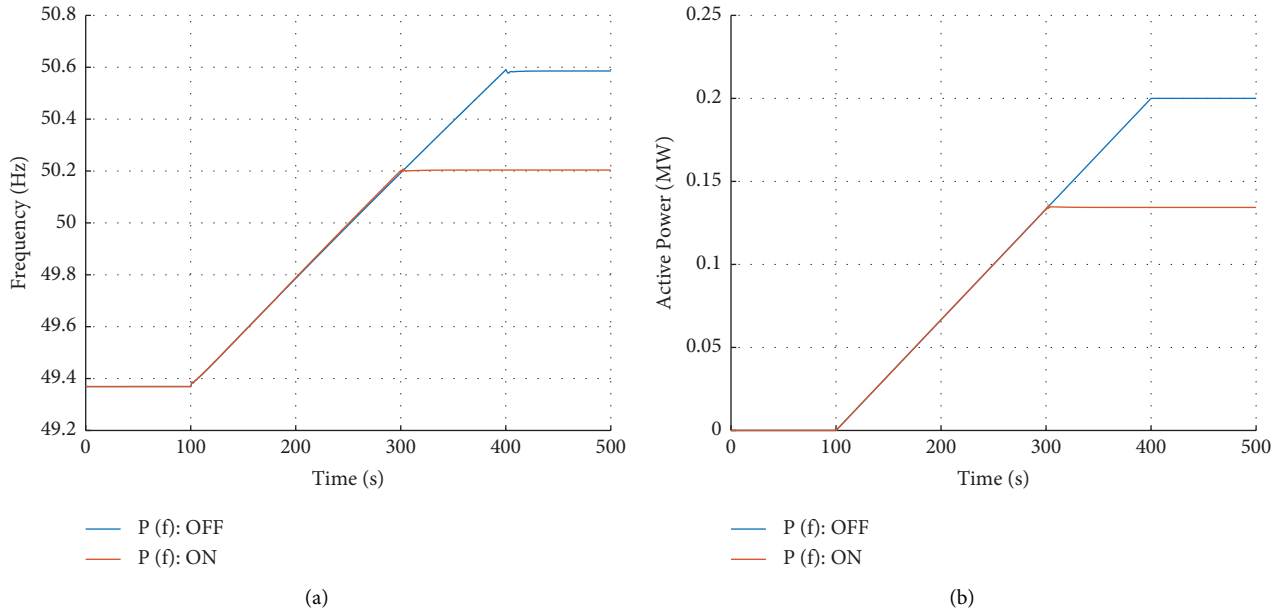

Figure 21: Frequency (a) and DG active power (b) when the $P(f)$ control logic is deactivated (blue) or activated (orange).

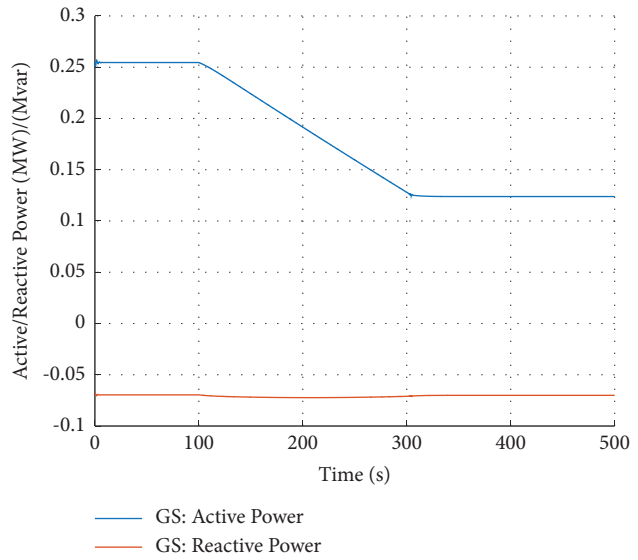

Figure 22: GS active (blue) and reactive (orange) power with $P(f)$ control logic activated.

stability limit of the capability curve. A similar behavior is seen on the active power profile (Figure 24): with the reconnection ramp, the active power of the DG unit reaches its nominal value (0.2 MW), reducing by the same amount, the active power produced by the GS.

Thus, numerical simulations demonstrated that the Q(V) control logic provides two benefits for the stability of the intentional electric island: firstly, the control logic brings the voltage value closer to the reference one for over/undervoltage events. Secondly, in overvoltage conditions,

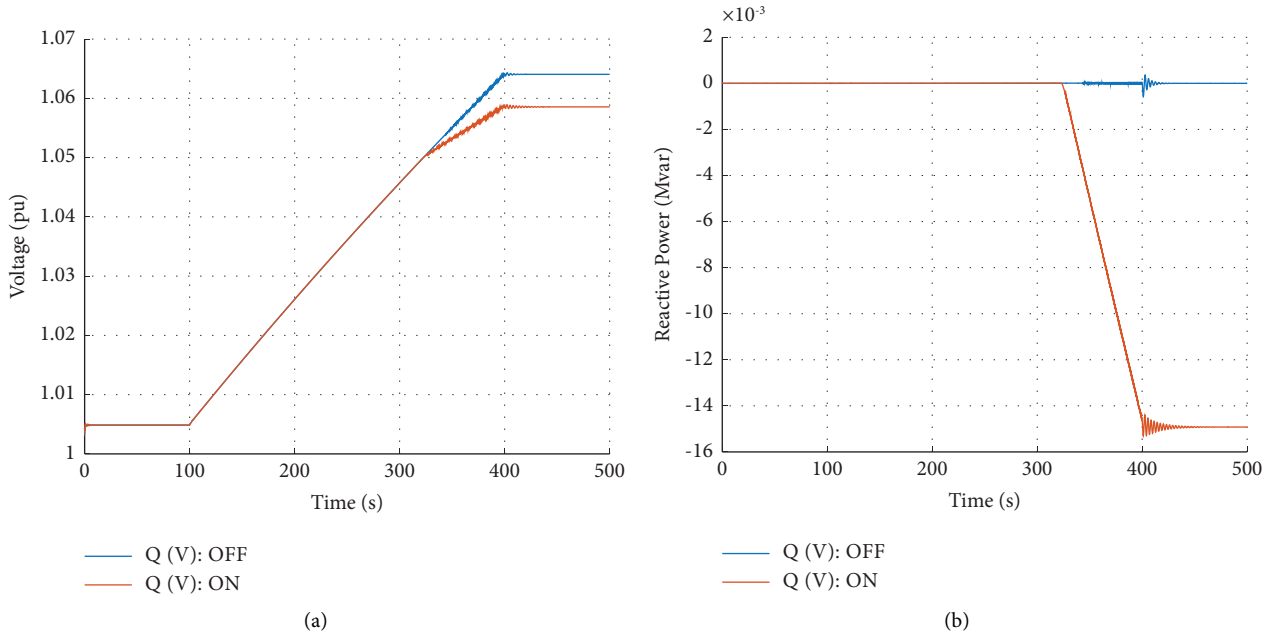

Figure 23: Voltage (a) and DG reactive power (b) when the Q(V) control logic is deactivated (blue) or activated (orange).

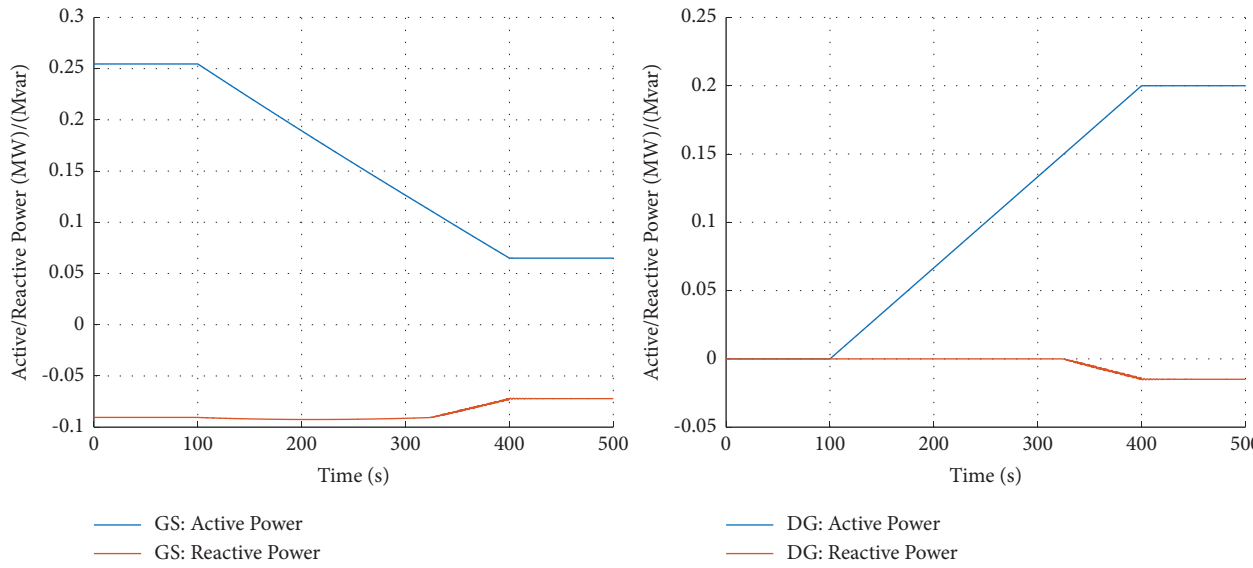

Figure 24: Active and reactive power profiles for GS and DG unit with the Q(V) control logic activated.

the GS operating point moves away from the stability limits toward the overexcited region of its capability curve.

6. Conclusions

The study carried out confirmed that the emergency supply of a portion of a public distribution grid with commercially available diesel-driven GenSets is, in most cases, practically feasible, thus improving the quality of service and reducing the outage periods. In particular, in areas in which most of the MV distribution grid is made by naked conductors, as rural or mountain areas, GSs can energize overhead lines even longer than 15 km without stability issues in any load condition. In urban environments, where usually the majority of lines are cables, the portion of the network that can be reenergized should not exceed a specific length (usually a few kilometers), depending on the size of the GS, the cross section of the cable line, the required power, and typology of the load. For this reason, other counterfeeding methods should be identified for these situations: for example, by changing the configuration of the system through the opening and closing control of MV disconnectors. Unstable conditions are more likely to emerge when loads are supplied close to the rated power of the GS (>90% P_n), especially if a droop characteristic is adopted for the speed governor.

Regarding the active network case study, particular attention must be paid to the amount of active power injected by the DG on the electric island, which must never exceed the one requested by the load. However, the control laws currently prescribed to DG units by ENTSO-E and Italian technical standards concerning the soft start ramp-up reconnection, $P(f)$ and Q(V), have shown not to interfere with the speed and voltage regulation of the GS. Indeed, they help the GS maintain the frequency and voltage inside the operating ranges, avoiding protection tripping.

Finally, although the current study has provided valuable guidelines for using GSs as emergency power supplies for improving the reliability and resilience of public distribution grids, even in the presence of DG units, there are still open questions that could motivate further research on the topic. Indeed, in addition to evaluating the effect on the island stability of different control laws of DG units and load typologies, future studies should focus on validating the results currently obtained by numerical models through experimental tests, also taking advantage of possible collaborations with DSOs.

Abbrevations

CEI: Comitato Elettrotecnico Italiano
DER: Distributed energy resource
DG: Dispersed generation
DSO: Distribution system operator
EU: European Union
GS: GenSet
LV: Low voltage
MV: Medium voltage
PLL: Phase-locked loop
PV: PhotoVoltaic
A_n: Rated apparent power
cos_{ref}: Reference cosine signal
D: Droop constant of the speed governor
EFD: Exciter output signal
EFD_{max}: Exciter maximum output
f: Frequency at the DG terminals
id_{ref}: Reference direct current signal
iq_{ref}: Reference quadrature current signal
J: Moment of inertia of the GenSet
K: Gain constant of the Q(V) control logic
K_a: Controller gain of the excitation system
K_{atc}: Actuator gain of the speed governor
K_e: Exciter constant
Lf_{max}: Maximum frequency value of the $P(f)$ control logic
LI: Lock-in active power value of the Q(V) control logic
LIf: Lock-in frequency value of the $P(f)$ control logic
LIp: Lock-in active power value of the $P(f)$ control logic
o_id: Start ramp-up signal of the DG unit
p: Active power signal of the DG unit
pi_max: Maximum active power of the DG unit before the activation of the P(f) control logic
P_{load}: Active power required by the load
P_m: Mechanical power
P_{max}: Maximum active power of the DG unit
P_n: Rated active power of the GenSet
P_{rated}: Rated active power required by the load
P_reg: Active power provided by the DG unit with P(f) control logic activated
Q_{load}: Reactive power required by the load
Q_{max}: Maximum reactive power exchanged by the DG unit
Q_{min}: Reactive power stability limit of the GenSet
Q_nr_pu: Nonregulated reactive power signal
Q_{rated}: Rated reactive power required by the load
Q_ref: Reference reactive power of the Q(V) control logic
sin_{ref}: Reference sine signal
T: Time constant of the Q(V) control logic
T_a: Armature time constant
TD: Combustion delay of the speed governor
T'_d: Transient time constant
T''_d: Subtransient time constant
T''_{do}: Open circuit time constant
TE: Excitation time constant
T_f: Stabilizer time constant
T_m: Mechanical torque
T_{max}: Maximum torque
T_{min}: Minimum torque
T_r: Measurement delay of the voltage excitation system
$T1$, $T2$, $T3$: Time constants of the electric control box of the speed governor
$T4$, $T5$, $T6$: Time constant of the actuator of the speed governor
u: Voltage signal of the DG unit
V: Voltage at the DG terminals
V_c: Steady-state voltage value at the GenSet terminals
V_f: Feedback voltage signal of the voltage exciter
V_{load}: Voltage measured at the load terminals
V_n: Rated voltage of the GenSet
V_{rmax}: Voltage controller output maximum
V_{rmin}: Voltage controller output minimum
$V1i$: Inner lower voltage threshold of the Q(V) control logic
$V1s$: Inner upper voltage threshold of the Q(V) control logic
$V2i$: Outer lower voltage threshold of the Q(V) control logic
$V2s$: Outer upper voltage threshold of the Q(V) control logic
X_d: Direct axis synchronous reactance
X'_d: Direct axis transient reactance
X''_d: Direct axis subtransient reactance
X_q: Quadrature axis synchronous reactance
X'_q: Quadrature axis transient reactance
X''_q: Quadrature axis subtransient reactance
$X0$: Zero sequence reactance
$X2$: Negative sequence reactance

yi_id: Input signal for direct axis current of the DG unit
yi_iq: Input signal for quadrature axis current of the DG unit
Z_{ref}: Reference impedance of the GenSet.

Data Availability

The data used to support the findings of this study are available from the corresponding author upon reasonable request.

Conflicts of Interest

The authors declare that there are no conflicts of interest regarding the publication of this paper.

Acknowledgments

The authors thank the Enel Group for generously providing access to the necessary datasheets and technical knowledge to support this research.

References

[1] GVR, *Generator Sets Market Size, Share & Trends Analysis Report by Fuel Type, by Power Rating (Low Power, Medium Power, High Power), by Application (Residential, Commercial, Industrial), by Region, and Segment Forecasts*, 2018.

[2] European Committee for Electrotechnical Standardization, *CENELEC European Standard EN 50160: Voltage Characteristics of Electricity Supplied by Public Electricity Networks*, European Committee for Electrotechnical Standardization, Netherlands, 2010.

[3] L. L. Schiavo, F. Villa, and C. Turconi, "Regulatory incentives for improving the resilience of electricity distribution grids in Italy," in *Proceedings Of the 25th International Conference on Electricity Distribution*, Madrid, Spain, 2019.

[4] Council of European Energy Regulators, *CEER: NRAs' Cooperation in Practice Status Review*, Council of European Energy Regulators, Strasbourg, France, 2016.

[5] ARERA, *Annex A to Resolution 566/2019/eel (TIQE 2020-2023): Code of the Output-Based Regulation of the Electricity Distribution and Metering Services for the Regulatory Period*, Turin, Italy, 2023, https://www.arera.it/it/docs/19/566-19.htm.

[6] D. Falabretti, L. Schiavo, S. Liotta, and A. Palazzoli, "A novel method for evaluating the resilience of distribution networks during heat waves," *International Journal of Electrical and Electronic Engineering & Telecommunications*, vol. 9, no. 2, pp. 73–79, 2020.

[7] ARERA, *Resolution 9 March 2017 127/2017/R/eel: Resilience of Electricity Transmission and Distribution Networks: Extension of Automatic Compensation to End Customers, paid by network operators*, Milan, Italy, 2017, https://www.arera.it/it/docs/17/127-17.htm.

[8] H. Laaksonen, H. Khajeh, C. Parthasarathy, M. Shafie-khah, and N. Hatziargyriou, "Towards flexible distribution systems: future adaptive management schemes," *Applied Sciences*, vol. 11, no. 8, p. 3709, 2021.

[9] Terna, *Scenario Description Document*, 2019, https://www.terna.it/it/sistema-elettrico/rete/piano-sviluppo-rete/scenari.

[10] E. Entso, *High Penetration of Power Electronic Interfaced Power Sources and the Potential Contribution of Grid Forming Converters*, Brussels, Belgium, 2020.

[11] D. Falabretti, F. Gulotta, and D. Siface, "Scheduling and operation of RES-based virtual power plants with e-mobility: a novel integrated stochastic model," *International Journal of Electrical Power & Energy Systems*, vol. 144, Article ID 108604, 2023.

[12] F. Gulotta, A. Rossi, F. Bovera et al., "Opening of the Italian ancillary service market to distributed energy Resources: preliminary results of UVAM project," in *Proceedings of the 2020 IEEE 17th International Conference on Smart Communities: Improving Quality of Life Using ICT*, IoT and AI (HONET), Charlotte, NC, USA, December 2020.

[13] Italian Electrotechnical Committee, *CEI 0-16: Reference Technical Rules for the Connection of Active and Passive Consumers to the HV and MV Electrical Networks of Distribution Company*, Italian Electrotechnical Committee, Italy, 2019.

[14] Italian Electrotechnical Committee, *CEI 0-21: Reference Technical Rules for the Connection of Active and Passive Users to the LV Electrical Utilities*, Italian Electrotechnical Committee, Italy, 2022.

[15] E. Entso, *ENTSO-E Network Code for Requirements for Grid Connection Applicable to All Generators*, 2013.

[16] E. Entso, *Implementation Guideline for Network Code "Requirements for Grid Connection Applicable to All Generators*, 2013.

[17] A. R. Cooper, D. J. Morrow, and K. D. R. Chambers, "Development of a Diesel Generating Set Model for Large Voltage and Frequency Transients," in *Proceedings of the IEEE Power and Energy Society General Meeting*, Minneapolis, MN, USA, July 2010.

[18] A. Renjit, M. Illindala, and D. Klapp, "Modeling and analysis of the CERTS microgrid with natural gas powered distributed energy Resources," in *Proceedings of the IEEE/IAS 51st Industrial & Commercial Power Systems Technical Conference*, I&CPS), Calgary, AB, Canada, May 2015.

[19] G. Papaioannou, I. Talavera, and J. Hanson, "The influence of diesel generators on frequency stability for isolated grids with high wind penetration," in *Proceedings of the International Conference on Renewable Energies and Power Quality*, Spain, March 2015.

[20] G. Papaioannou, M. Fleckenstein, and H. Zimmer, "Dynamic Frequency Controlling for Isolated Island Power System," in *Proceedings of the Electrimacs*, Valencia, Spain, May 2014.

[21] A. Renjit, M. Illindala, and D. Klapp, "Graphical and analytical methods for stalling analysis of engine generator sets," *IEEE Transactions on Industry Applications*, vol. 50, no. 5, pp. 2967–2975, 2014.

[22] A. Moeini, A. Darabi, S. Rafiei, and M. Karimi, "Intelligent islanding detection of a synchronous distributed generation using governor signal clustering," *Electric Power Systems Research*, vol. 81, no. 2, pp. 608–616, 2011.

[23] Y. A. Elshrief, A. D. Asham, B. Bouallegue et al., "An innovative hybrid method for islanding detection using fuzzy classifier for different circumstances including NDZ," *Journal of Radiation Research and Applied Sciences*, vol. 15, no. 2, pp. 129–142, 2022.

[24] D. Mlakic, H. R. Baghaee, and S. Nikolovski, "A novel ANFIS-based islanding detection for inverter-interfaced microgrids," *IEEE Transactions on Smart Grid*, vol. 10, no. 4, pp. 4411–4424, 2019.

[25] A. K. Ozcanli and M. Baysal, "Islanding detection in microgrid using deep learning based on 1D CNN and CNN-LSTM networks," *Sustainable Energy, Grids and Networks*, vol. 32, Article ID 100839, 2022.

[26] K. Gottapu, T. R. Jyothsna, and V. N. Yirrinki, "Performance of a new hybrid approach for detection of islanding for inverter-based DGs," *Renewable Energy Focus*, vol. 43, pp. 1–10, 2022.

[27] S. Nikolovski, H. R. Baghaee, and D. Mlakic, "Islanding detection of synchronous generator-based DGs using rate of change of reactive power," *IEEE Systems Journal*, vol. 13, no. 4, pp. 4344–4354, 2019.

[28] D. Mlakic, H. R. Baghaee, and S. Nikolovski, "Gibbs phenomenon-based hybrid islanding detection strategy for VSC-based microgrids using frequency shift, $THD," *IEEE Transactions on Smart Grid*, vol. 10, no. 5, pp. 5479–5491, 2019.

[29] H. R. Baghaee, D. Mlakic, S. Nikolovski, and T. Dragicevic, "Anti-islanding protection of PV-based microgrids consisting of PHEVs using SVMs," *IEEE Transactions on Smart Grid*, vol. 11, no. 1, pp. 483–500, 2020.

[30] H. R. Baghaee, D. Mlakic, S. Nikolovski, and T. Dragicevic, "Support vector machine-based islanding and grid fault detection in active distribution networks," *IEEE Journal of Emerging and Selected Topics in Power Electronics*, vol. 8, no. 3, pp. 2385–2403, 2020.

[31] F. Tooryan and E. R. Collins, "Optimum size and placement of distributed generators in microgrid based on reliability concept," in *Proceedings of the 2018 IEEE Power and Energy Conference at Illinois*, PECI), Champaign, IL, USA, February 2019.

[32] A. Alassi, K. Ahmed, A. Egea-Alvarez, and O. Ellabban, "Performance evaluation of four grid-forming control techniques with soft black-start capabilities," in *Proceedings of the 2020 9th International Conference on Renewable Energy Research and Application*, ICRERA), Glasgow, UK, September 2020.

[33] F. Sadeque, D. Sharma, and B. Mirafzal, "Multiple grid-forming inverters in black-start: the challenges," in *Proceedings of the 2021 IEEE 22nd Workshop on Control and Modelling of Power Electronics (COMPEL)*, Cartagena, Colombia, November 2021.

[34] T. Ali, D. Florian, and K. Friederich, "Grid-forming converters – inevitability, control strategies and challenges in future grids application," in *Proceedings of the CIRED 2018 Ljubljana Workshop on Microgrids and Local Energy Communities*, Ljubljana, June 2018.

[35] A. Paquette, M. Reno, and R. Harley, "Causes of unequal transient load sharing in islanded microgrid operation," *IEEE Industry Applications Magazine*, vol. 23, 2014.

[36] T. L. Vandoorn, B. Meersman, J. D. M. De Kooning, and L. Vandevelde, "Directly-coupled synchronous generators with converter behavior in islanded microgrids," *IEEE Transactions on Power Systems*, vol. 27, no. 3, pp. 1395–1406, 2012.

[37] M. Z. Kreishan, G. P. Fotis, V. Vita, and L. Ekonomou, "Distributed generation islanding effect on distribution networks and end user loads using the load sharing islanding method," *Energies*, vol. 9, no. 11, p. 956, 2016.

[38] J. Grainger, W. Stevenson, and G. Chang, *Power System Analysis*, Mc Graw Hill, New York, USA, 2016.

[39] V. Carrescia, *Generating Sets*, Edizioni TNE, Turin, Italy, 2020.

[40] P. Neuman, "Island operations of electric generators connected to one substation," *Transactions on Electrical Engineering*, vol. 6, no. 2, 2017.

[41] E. Distribuzione, *Guide for the Connection to the Electricity Grid of Enel Distribuzione*, 2021, https://www.e-distribuzione.it/connessione-alla-rete/Regole_tecniche.html.

[42] O. Fahmy, A. Attia, and M. Badr, "A novel analytical model for electrical loads comprising static and dynamic components," *Electric Power Systems Research*, vol. 77, no. 10, pp. 1249–1256, 2007.

[43] S. Chakrabarti, "Static load modelling and voltage stability indices," *International Journal of Power and Energy Systems*, vol. 29, no. 3, 2009.